Available online at www.sciencedirect.com
SCIENCE DIRECT®
Combustion and Flame 137 (2004) 148–162
Combustion and Flame
www.elsevier.com/locate/jnlabr/cnf

Experimental study of the combustion dynamics of jet fuel droplets with additives in the absence of convection

J.H. Bae and C.T. Avedisian *

Sibley School of Mechanical and Aerospace Engineering, Cornell University, Ithaca, NY 14853-7501 USA

Received 23 July 2003; received in revised form 4 February 2004; accepted 4 February 2004

Abstract

Combustion of stationary JP8 fuel droplets mixed with additives is examined in a low gravity environment to reduce the influence of convection and promote spherical droplet flames. Both qualitative information on flame structure and sooting tendencies and quantitative information on evaporation rates and flame and soot shell diameters are reported. The additives were hexanol ($C_6H_{14}O$) and a commercial blend of a detergent/dispersant termed "+100" that is widely used as an additive in military transport systems. Experiments for pure nonane (C_9H_{20}) and hexanol droplets are also reported for comparison with single component fuels that have boiling points close to JP8. Nonane was also used for calibrating the experimental design. +100 is a commercial additive developed for JP8 to improve its thermal stability in trace quantities but its influence on combustion is essentially unknown. The hexanol concentration in JP8 was fixed to correspond to about 0.078 mass fraction of oxygenate in the JP8 + hexanol mixture and the +100 concentration in JP8 was set at the commercial value (256 ppm). The initial droplet diameters for quantitative analyses were kept within a narrow range (0.40 to 0.52 mm) to eliminate consideration of the effect of initial droplet diameter in the interpretation of the results. Experiments were carried out in an oxidizing ambience containing either 79% nitrogen inert or 70% helium inert, the latter to compare results for burning under conditions where soot formation was suppressed. The lower concentration of helium inert was necessitated to allow ignition by the multiple spark arrangement used in the present investigation.

Extensive droplet heating was observed for JP8 and JP8 + 100 in air. JP8 + hexanol, along with pure nonane and hexanol, showed no evidence of droplet heating due to the lower thermal diffusion time associated with the higher thermal diffusivity of hexanol and nonane compared to JP8. The burning rate was dependent on time for burning in both air and the 70% He/30% O_2 mixture in which soot formation was virtually eliminated. Some evidence for sooting propensities in the approximate order JP8 > JP8 + 100 > JP8 + hexanol was found by comparing backlighted and flame-illuminated photographs. A scaling relationship is presented that consolidates the droplet, flame, and soot shell diameters into a single curve with a power law relationship of the nondimensional burning time.

Keywords: Jet fuel; JP8; Soot; Microgravity; Droplet combustion; Additives

1. Introduction

JP8 is the most widely used liquid fuel for power and propulsion in commercial and military transport systems. It is a kerosene derivative composed of a large number of constituents that encompass a wide range of boiling points, sooting tendencies, and heats of vaporization [1]. JP8 serves a dual purpose. It is a fuel in its own right, and at the same time it is the primary coolant for aircraft hydraulics, engines, and environmental control systems [2,3]. As such, the performance of JP8 is measured in terms of its non-

* Corresponding author.
E-mail address: cta2@cornell.edu (C.T. Avedisian).

0010-2180/$ – see front matter
doi:10.1016/j.combustflame.2004.02.003

Nomenclature

D	Droplet diameter
Gr	Grashof number
K	Burning rate
k	Thermal conductivity
Pr	Prandtl number
Re	Reynolds number
Sp	Sphericity number
T	Temperature
t	Time
Y	Mass fraction
α	Thermal diffusivity
τ	Characteristic time

Subscripts

b	Burnout
c	Convection
d	Droplet
df	Diffusion
f	Flame
g	Gas phase
l	Liquid phase
O_∞	Oxygen in gas ambience
o	Initial state
s	Soot shell
∞	Gas ambience

combustion tasks and its effectiveness as an efficient fuel.

Prior research to improve JP8 has centered around its role as a coolant to improve thermal stability. This effort led to development of an additive consisting of blend of a detergent/dispersant (Betz 8Q405, 27.3% (volume percent)), butylated-hydroxyl-toluene (BHT, 9.8%), metal deactivator (MDA, 1.2%), and solvent oil (61.7%) at 256 ppm in JP8. This additive is termed "+100" [2,3]. At the same time, surprisingly little is known about how +100, or other additives for that matter, influences droplet combustion of JP8. The present study examines this aspect.

We present here new data on the combustion dynamics of JP8 droplets blended with +100 and hexanol ($C_6H_{14}O$). Specific aspects investigated include the evolution of the droplet, flame, and soot dynamics and how hexanol and +100 influenced these quantities; the sooting propensities of JP8 with +100 and hexanol; and the development of a scaling relationship to consolidate the measurements. Hexanol was chosen as an additive because it has a boiling point close to the range of boiling points of the JP8 constituents at which microexplosions [4] are not expected to occur;[1] it has a low propensity for water absorption and a higher liquid thermal diffusivity than JP8 which will reduce the droplet heating period; and the reduced sooting tendency of hexanol compared to JP8 was expected to produce observable differences in soot dynamics of JP8 + hexanol compared to JP8. In addition to JP8 and hexanol, some results for pure nonane are reported because nonane droplets were used to calibrate the fiber-supporting design with a free droplet method, which is described in Section 2. The initial droplet diameters ranged from 0.40 to 0.52 mm. This small range was not expected to influence soot formation [5,6]. For practical purposes the results described in this paper may be considered as pertaining to a unique initial droplet diameter in this range.

Because of the multicomponent nature of JP8 and the complex burning process it was expected to undergo, we carried out the experiments in an ambience that promoted gas-phase spherical symmetry, which is to say microgravity. In such an environment, a spherical flame is formed because of the one-dimensional gas-phase transport process and the sooting dynamic is tractable with soot aggregates being trapped in a spherical "shell" surrounding the droplet [7,8]. Fig. 1 is a schematic of this burning configuration.[2]

No prior research on spherical droplet flames of JP8 has been carried out. On the other hand, droplet combustion of JP8 in a strong convective field has been previously studied. Convection was generated during free-fall of droplets in an isothermal vertical furnace [11] (forced convection) or burning of suspended JP8 droplets in a quiescent ambience at

[1] For this reason, we did not study lower alcohols such as methanol or ethanol. Methanol was not fully miscible in JP8 and our preliminary testing showed that JP8/ethanol mixtures exhibited microexplosions.

[2] Conditions are never as perfect as depicted in Fig. 1. For example, the soot shell rarely remains intact throughout combustion because as the soot aggregates grow their stability at the trapped position drops [9] and it is easy for small perturbations of the burning process to initiate drifting of the agglomerates away from the droplet. Internal liquid circulation can also exist due to artifacts of the droplet deployment process [10] that will not be self-evident simply from noting the state of gas-phase symmetry. In our work we are using the term "spherically symmetric" to mean essentially the outward appearance of such, recognizing the above limitations.

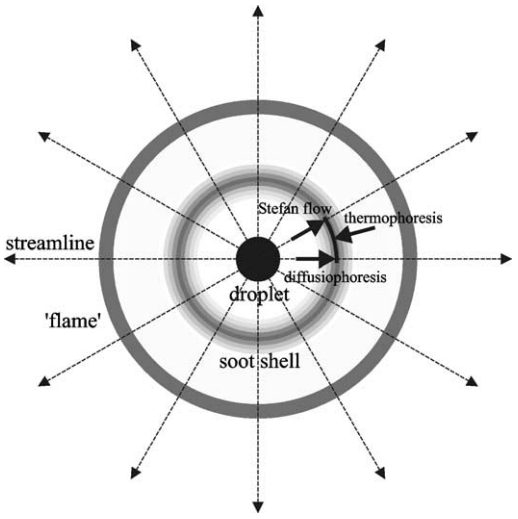

Fig. 1. Schematic representation of idealized spherical symmetry for droplet burning.

Earth's normal gravity (buoyancy induced flow) [12]. The convective flow produces wake flames with long tails through which soot is transported by convection. The information reported in the present work complements these studies by providing data at the other extreme of essentially a zero relative velocity between the droplet and the ambience.

For a fuel as complex as JP8 with its variability of composition (due to manufacturing standards), there are advantages to studying the burning process from the perspective of Fig. 1: JP8 soots extensively; its multicomponent nature increases the potential for microexplosions which can limit the range of the data; and preferential vaporization could occur which could challenge the interpretation of the data by the difficulty of knowing precisely which species have a dominant role in this process. As a fuel, JP8 is at the other end of the spectrum of a miscible binary fuel blend such as the nonane/hexanol mixture [13] which was shown to burn without any of these complex processes present. The present study demonstrates the extent to which spherical symmetry can provide benchmark data for fuel characterization and analysis of a complex fuel system like JP8, as it has been well known to do for ideal fuel systems.

There is also another reason relevant to applications for examining spherical symmetry for burning of isolated JP8 droplets besides the fundamental understanding it provides. It is that models for processes at the droplet level are very important in spray analysis. The burning rate, K_c, is typically expressed in terms of a correction for convection as $K_c = K[1 + f(Re, Pr)]$ (Refs. [14] and [15] provide excellent reviews of models for the influence of convection on droplet burning rate and the interrelationship of these models with spray models). The consistency of such correlations depends on recovering the correct value of K in the limit as $Re \to 0$ wherein $K_c \to K$ (the case in Fig. 1). Such correlations can only be used if K is known. Because the quasi-steady state model of droplet burning is not applicable to a fuel like JP8 which has burning characteristics not included in the basic model, direct measurement of K is required.

For the present experiments, the ambient gas was a blend of oxygen with an inert, nitrogen or helium: 21% oxygen (mole percent) in 79% nitrogen (air), and 30% oxygen in 70% helium. The higher oxygen concentration in helium was required because of difficulty in spark-igniting the test droplets at lower oxygen concentrations. Droplet burning in the 70% He/30% O_2 mixture was included for two reasons. It would identify the role of soot formation on the various combustion parameters since in helium sooting tendencies would be greatly reduced, and the higher helium gas thermal conductivity relative to nitrogen would alter heat transfer to the droplet and thereby the droplet burning dynamics, principally the evolution of droplet diameter and the initial droplet heating period.

The +100 concentration was selected to correspond to the commercial loading (256 ppm or 0.0256 vol%). This is an extremely low concentration yet it has been shown to significantly improve thermal stability of JP8 [2,3]. A concentration at this loading was not expected to influence soot formation. For example, diesel fuels blended with methanol show measurable reductions in soot formation only above 80% methanol [16]; toluene droplets blended with methanol show nonluminous flames above 75% methanol loading [17]; and for 25% hexanol in 75% nonane, soot shells were not formed in nonane/hexanol droplet flames [13]. It would be remarkable if +100 mixed at 0.0256% had any impact on sooting tendencies. The present study examines this issue and presents some qualitative information.

The hexanol concentrations were selected to give oxygenate loadings in JP8 that would be considered reasonable from an industrial standpoint. Additives at less than about 0.10 mass fraction of oxygenate are viable for industrial use [18]. Using this as a baseline, we selected a 50% volume fraction concentration of hexanol in JP8 which corresponds to an oxygenate mass fraction of 0.078 for JP8 + 50% hexanol.

A high-speed 16-mm movie camera was used to record the droplet burning process. Black and white film with backlighting provided quantitative data on droplet, soot shell, and luminous zone diameters and qualitative information on sooting tendencies. Color film with no backlighting recorded flame structure and provided additional insights on

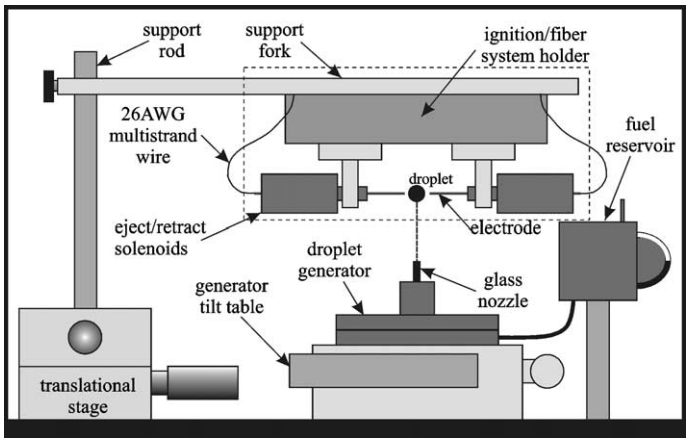

Fig. 2. Schematic diagram of apparatus (side view, not to scale) showing droplet deployment arrangement, electrodes, and positioning devices. Fig. 3 shows greater detail of components within the dotted line.

sooting tendencies. Care was taken to keep the backlighting intensity, ambient conditions, and ignition mechanism identical to allow a valid basis of comparison of sooting tendencies from among the photographs taken. Backlighted photography is an acceptable qualitative tool under these circumstances. Some past work has also examined relative sooting trends of jet fuel droplets burning in a highly convective environment by assessing luminosity trends from flame-illuminated images [11] with good success.

2. Experimental design and measurements

The experiments were carried out in a low gravity environment to promote spherical droplet flames. A low gravity was achieved using a drop tower facility, which was 7.6 m in height providing about 1.2 s for an experimental duration [13,19]. The experimental time was more than adequate to observe the complete burning history for the droplet sizes examined. Gravity levels were less than 10^{-4} of Earth's gravity ($9.8\ \mathrm{m/s^2}$) which corresponds to a sphericity number,[3] *Sp*, or Grashof number, *Gr*, in the range where spherical droplet flames are expected [6,20].

The general procedure of the experiments was to position a droplet at the desired location where cameras were focused. Then, the droplet and its sealed surroundings and associated hardware were put into free-fall. During the downward flight of the instrumentation package, the droplet was ignited and the ignition source was withdrawn to provide an unobstructed ambience for the combustion process. We used a new fiber design for droplet mount because of its greater ease of operation compared to a free droplet (previously used designs for droplet deployment in low gravity are reviewed in Ref. [21]). We calibrated our particular fiber support design against free nonane droplets under identical conditions of ignition and ambient gas to ensure that the fiber did not influence the burning process as is shown in Fig. 4 later.

A schematic of the fiber support arrangement is shown in Figs. 2 and 3. It consisted of an aluminum ring to hold four vertical posts for mounting very small 12-μm-diameter SiC fibers and four solenoid actuators whose plungers were attached to the electrodes used for spark ignition. The two fibers were crossed at an angle of 120° and a test droplet was mounted at the intersection to prevent the droplet from sliding along a fiber during combustion. We experimented with different viewing directions. For the one shown in Fig. 3, the flame/fiber interaction will produce a "glow" from the fiber for the 16-mm camera viewing direction which is outside of the region of the droplet and soot shell. The advantage here is that visibility of the droplet or soot shell will not be obstructed by the fiber glow. At the same time, for the CCD video viewing direction which is at 90° from the 16-mm camera shown in Fig. 3, the "glow" will appear inside the flame boundary. The advantage here is that the flame boundary is not obstructed by the fiber glow from this direction (which is good for making measurements of flame diameter). We occasionally interchanged the 16-mm camera and video viewing directions. It must be understood that the photographs (discussed in Section 3.1) which show a fiber glow across the flame correspond to the direction of the 16-mm movie camera in Fig. 3, and those where the glow

[3] $Sp \approx Pr\sqrt{Gr_{\mathrm{Df}}/\ln(1+Y_{\mathrm{O}_\infty})}$ where Pr, Gr_{Df}, and Y_{O_∞} are Prandtl number, Grashof number based on flame diameters, and ambient oxygen mass fraction, respectively.

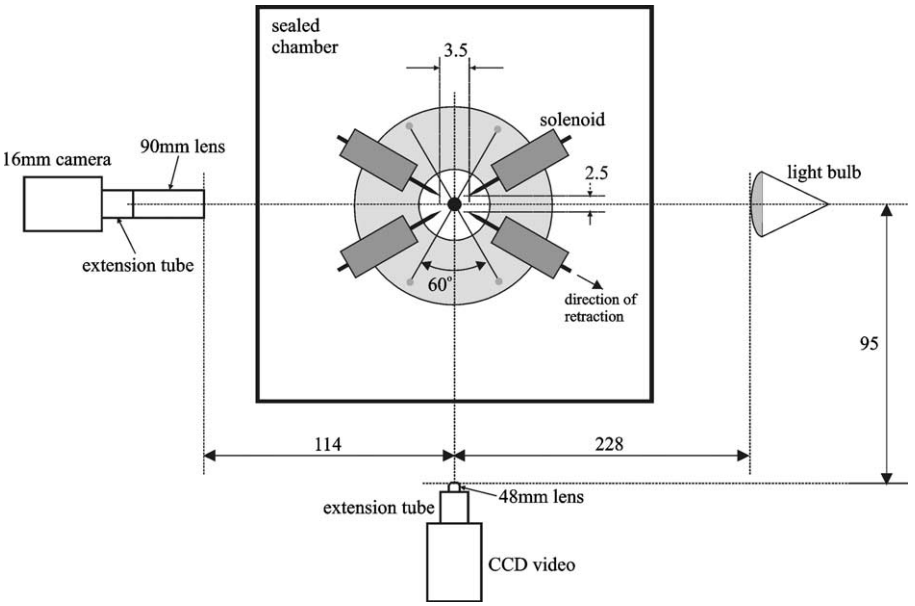

Fig. 3. Detail schematic of fiber mount (bottom view, not to scale) showing placement of electrodes, camera lenses, and light source. Distances are in millimeters.

is inside of the droplet are in the direction of the video camera.

Test droplets were mounted on the fibers by essentially "shooting" a droplet formed from a piezoelectric generator [19] onto the intersection of the two fibers. Droplets of the desired size were created by successive impingements and coalescence events. We could control the initial droplet diameter to the desired values which was in the range of 0.40 to 0.52 mm for the present study.

Droplets were ignited by two sparks positioned on opposite sides of the droplet from four electrodes. The placement of the electrode tips from the droplet was crucial for reliable ignition. Fig. 3 gives dimensions. The spark duration was 0.8 ms and the electrodes were immediately retracted away from the droplet. The sparks were activated 320 ms after the period of low gravity commenced in order to allow vibrations to subside that were induced by the physical separation of the instrumentation package from the electromagnet which held the package in place.

Both black and white 16-mm movies and color 16-mm movies were taken using a LOCAM II high-speed movie camera using a 90-mm Olympus Zuiko lens fitted with a 100-mm extension tube. For the black and white movies (using Kodak 7278 film), we used f4.0, a framing rate of 200 frames/s, and a shutter speed of 1/450 s; for the color movies (Kodak 7251 film) we used f2.0, a framing rate of either 50 frames/s with a shutter speed of 1/100 s in air or 15 frames/s with a shutter speed of 1/36 s in the 70% He/30% O_2 mixture. Color video images were taken with a COHU 8295 CCD camera fitted with a Bausch and Lomb 48-mm 0.08 objective lens and 80-mm extension tube for flame diameter measurements. The placement of the lenses relative to the droplet is illustrated in Fig. 3. Both self-illuminated movies (via the flame luminosity) and backlighted movies were used. Backlighting was provided by a GE FHX 25-W halogen lamp (what we will call "low intensity" lighting) or a GE ENG 300-W projector bulb (what we will call "high intensity" backlighting). High intensity was used for JP8 to overcome problems with visibility associated with soot formation and low intensity was used for hexanol and nonane.

Quantitative measurements of droplet and soot shell diameter were made by transporting each image from the 16-mm movie film (scanned with a Microtex 3900 DPI scanner) or video to a PC for analysis by Media Cybernetics ImagePro Plus 4.0 software.

Semiquantitative measurements were made of the amount of soot formed. This was accomplished by first identifying a region around the droplet within which the analysis software scanned across pixels contained in the box. The box was typically a square and its size was fixed for droplets in a given series. An average pixel intensity was determined within the box by the software using a fixed gray scale threshold set by the user. The relative amount of soot formed from among different droplets blends was determined by the average intensity value within the box, the higher value implying more soot formation. This ap-

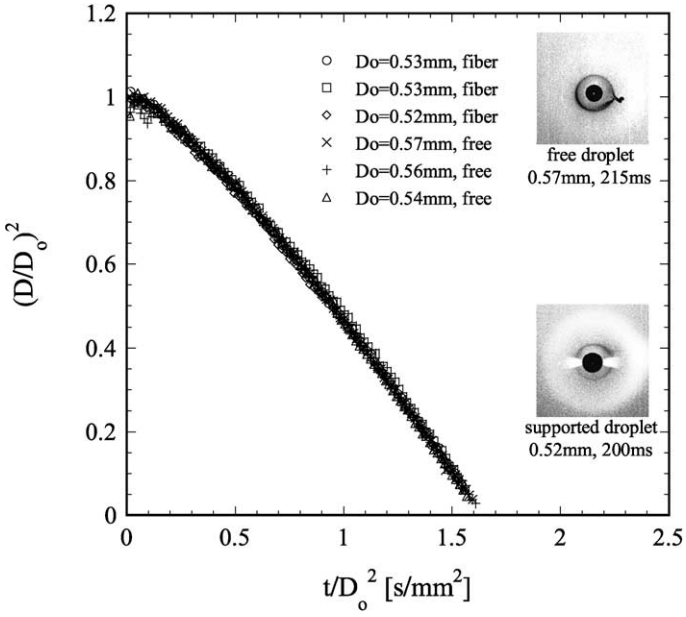

Fig. 4. Evolution of droplet diameter for free and fiber supported for nonane droplets of the indicated diameter. (Insets) Selected photograph illustrating configurations of free and fiber-supported nonane droplets. Fiber "glow" for the fiber-supported droplet is shown which is due to flame/fiber interaction. The tail on soot cloud for the free droplet is due to residual convection.

proach was found to coincide with more subjective judgments made by eye of the visual record of the droplet burning process.

Since JP8 is highly sooting, accumulation of soot aggregates in a shell was expected to be a prominent feature of the burning process. In fact, it was so excessive that it compromised data quality by obscuring portions of the droplet for some of the conditions examined. When the droplet was not visible over its entire circumference because of this problem, we attempted to complete the arc of the circle if four or more points on the boundary could be seen. Otherwise, the movie frame was discarded. This procedure left gaps in some of the D^2 progressions as will be apparent when the measurements are discussed. Regarding the "flame" diameter in air, it was taken as the outer zone of the yellow luminous boundary on the color video frames. For burning in the 70% He/30% O_2 mixture the flame color was mostly blue and the outer blue zone was taken as the flame boundary.

Data from fiber-supported droplets using the apparatus described previously were compared to a free-floating droplet using a design described previously [4–6,19]. The droplet diameter is the most accurate measurement we can make (as contrasted with the soot shell or flame diameter) so it was used as the benchmark. Fig. 4 shows the evolution of droplet diameter for a series of fiber-supported and free-floating nonane droplets. The diameter progressions are virtually indistinguishable between the two burning configurations which demonstrate the validity of the fiber design. Interestingly, the very small fibers we used still influenced the soot dynamics as soot particles often attached to the fiber as burning progressed. However, the unusual patterns of soot trapping associated with very large fibers were never seen [22] with these 12-μm-diameter fibers.

Soot aggregates were collected from deposits on the fiber and photographed by transmission electron microscopy (TEM). Mean aggregate sizes were measured from the TEM negatives using the aforementioned image analysis software.

3. Discussion

3.1. High-speed movie visualizations

Fig. 5 shows selected flame-illuminated images from 16-mm color movie sequences which compare nonane, JP8, JP8 + 100, JP8 + hexanol, and pure hexanol. The photographs show the most intense flame image for the respective series as determined by the software analysis package. In this way, qualitative trends in flame emission and sooting tendencies could be compared. The times at which the photographs were taken are indicated beneath each picture. It is evident that the hexanol flame luminosity (Fig. 5e) is the least intense compared to the other fuels, which shows its comparatively nonsooting tendency. Flame

(a) JP8 $Do \sim 0.62$ mm $t = 140$ ms | (b) JP8 + 100 $Do \sim 0.60$ mm $t = 140$ ms | (c) JP8/50% hexanol $Do \sim 0.51$ mm $t = 160$ ms | (d) Nonane $Do \sim 0.55$ mm $t = 200$ ms | (e) Hexanol $Do \sim 0.58$ mm $t = 270$ ms

Fig. 5. Selected color images of flame-illuminated photographs comparing flame luminosity of the fuels burning in air. Images show the brightest flames from the sequences.

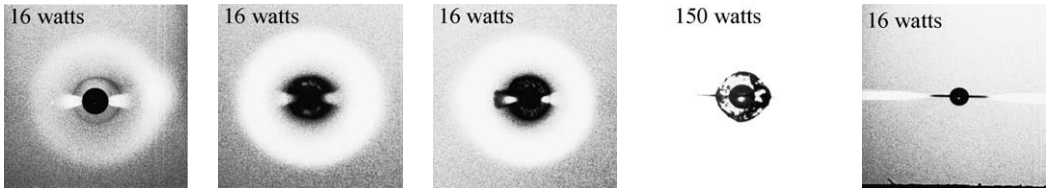

(a) Nonane $Do \sim 0.52$ mm $t = 200$ ms | (b) JP8 $Do \sim 0.50$ mm $t = 170$ ms | (c) JP8 + 100 $Do \sim 0.52$ mm $t = 170$ ms | (d) JP8 + 100 $Do \sim 0.45$ mm $t = 165$ ms | (e) Hexanol $Do \sim 0.52$ mm $t = 235$ ms

Fig. 6. Backlighted photographs of selected frames of JP8 and nonane droplets burning in air (a)–(c) showing effect of low backlight intensity on droplet and soot shell visibility. Frames are of the darkest soot images in the series. (d) Photograph using "high intensity" backlighting. (e) Hexagonal droplet burning without soot shell.

luminosity differences between JP8 and JP8 + 100 are indistinguishable.

Fig. 6 shows selected black and white photographs using low intensity lighting of nonane, JP8, JP8 + 100, and hexanol droplets. The initial droplet diameters were again the same. As with Fig. 5, the photographs in Fig. 6 were chosen from the most intense images in the movie sequences from which they were obtained. The droplet, soot shell, and flame boundary for the nonane droplet (Fig. 6a) are all visible. Differences of sooting tendencies between JP8 and JP8 + 100 are again not discernible from the photographs shown in Figs. 6b and 6c. Droplet visibility is poor for JP8 and JP8 + 100 where soot accumulation is excessive compared to nonane (Fig. 6a) or hexanol (Fig. 6e). With high intensity backlighting (Fig. 6d), the droplet and soot structure are now both visible though there is still some obscuration of the droplet by soot accumulation in the shell. This concern posed some challenges of data acquisition as noted previously.

Fig. 7 compares backlighted images of JP8, JP8 + hexanol, JP8 + 100, and JP8 + 100 + hexanol droplets burning in air. The times of the photograph after ignition and the initial droplet diameter are given beneath each picture. The selected frames are of the most intense (i.e., darkest) images from the individual burning records. As shown in Figs. 7a and 7b, soot accumulation obscures part of the JP8 and JP8 + 100 droplets, but with hexanol addition it is much less. There appears to be less soot accumulation for JP8 + 100 compared to JP8, where we differentiate between "accumulation" and "formation."[4] It is important to note that we do not know how much soot actually forms in the droplet flame because we have not measured soot volume fraction. Nevertheless, because backlight intensity was identical for all images reported here, differences in image darkness indicate differences in the amount of soot formed. On this basis, Fig. 7 would suggest that soot propensities are in the order JP8 > JP8 + 100 > JP8(+100) + hexanol.

The effect of hexanol mixed with JP8 on soot formation, shown in Figs. 7c and 7d, is understood to be a consequence of oxygen (bound in hexanol) inhibiting reactions leading to soot formation [16]. The effect is largely one of dilution because of the high hexanol concentration (50%). For +100 in a much smaller amount, 256 ppm, a dilution influence on soot formation is unlikely; yet Figs. 7a and 7b suggest that +100 does inhibit soot formation.

We investigated further this influence of +100 on soot by carrying out experiments in oxygen/helium

[4] Soot formation is the transformation of precursor particles into opaque and agglomerated spherical monomers whose size ranges from 50 nm down to 10 nm [23]. Soot accumulation is defined here as the progressive build-up of aggregates between the droplet and the flame where they are trapped to form the soot shell [21].

(a) JP8 $Do \sim 0.49$ mm $t = 300$ ms

(b) JP8 + 100 $Do \sim 0.45$ mm $t = 230$ ms

(c) JP8 + 50% hexanol $Do \sim 0.48$ mm $t = 195$ ms

(d) JP8 + 100 + 50% hexanol $Do \sim 0.47$ mm $t = 185$ ms

Fig. 7. Selected high intensity backlighted photographs of JP8 droplets burning in air showing effect of +100 and hexanol addition on soot accumulation. Frames are of the darkest soot images in the series.

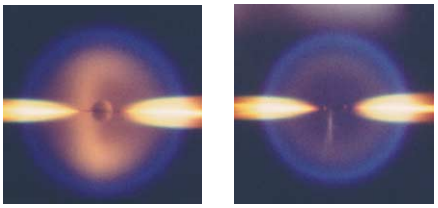

(a) JP8 $t = 133$ ms

(b) JP8 + 100 $t = 66$ ms

Fig. 8. Photographs of JP8 droplet flames in the 70% He/30% O_2 mixture. Initial droplet diameter is 0.50 mm. Images show the brightest flames from the sequences. JP8 + 100 (b) has a fainter yellow emission compared to JP8 (a).

mixtures, specifically 70% He/30% O_2. Fig. 8 shows selected images of the most intense self-illuminated flames of JP8 and JP8 + 100 droplets in their respective sequences. The time after ignition is indicated beneath each of the photographs and the initial droplet diameters were the same. The JP8 droplet flame (Fig. 8a) has an outer blue zone with a visible yellow core of apparently greater image intensity than the JP8 + 100 (Fig. 8b) droplet flame, which is almost entirely blue. This indicates more soot being formed for JP8 compared to JP8 + 100. Generally, a helium inert would be expected to reduce soot formation by a combination of a lower flame temperature and higher average gas-phase mass diffusivity which influences the combustion chemistry and residence time of molecules between the droplet and the flame [24].

It is interesting that with +100 blended in JP8 at 256 ppm, soot formation seems to be reduced as shown in Figs. 7 and 8. Instead of a dilution effect, there could be a chemical effect. Previous studies [25–28] showed that even in trace amounts (< 1% according to Ref. [28]), certain additives can influence soot formation by their ability to chemically catalyze oxidation of soot. For example, Bonczyk [27] showed that adding ferrocene in trace amounts reduces soot at a late stage of combustion by catalytic action of Fe_xO_y. Now the concentration of the +100 additive in JP8 we have considered is far higher compared to the metal additives typical of these previous studies. As a result, it would not be surprising that the constituents of +100 could conceivably promote a catalytic effect similar to that of metal additives in trace quantities. Precisely what that chemistry would be needs further study.

Another possible mechanism for an influence of additives on soot formation even in trace quantities is its influence on thermofluid properties, for example, surface tension (as for a surfactant) or viscosity, and thereby liquid transport when internal circulation is present inside the droplet (i.e., Marangoni convection when temperature gradients exist). Liquid motion in the droplet will influence transport of species to the surface and the rate of transport is in turn determined by the liquid's viscosity and surface tension. That the JP8 flame is noticeably more luminous than JP8 + 100 in Fig. 8, thus indicating greater soot formation, could be evidence of enhanced liquid transport to the surface of chemical species in the JP8 blend which will more readily form soot precursor species. The burning conditions are ostensibly designed to minimize internal circulation but may not have completely eliminated it.

We were able to harvest some soot aggregates from JP8 droplets for TEM analysis. Aggregates were collected from material that had been deposited on the support fiber. TEM images of JP8 soot aggregates appear to be connected by individual elements which have a spherical or near spherical shape, which is similar to the images of other studies [23]. Measurements of these individual aggregates averaged 60 nm with a large standard deviation of ± 20 nm. Dobbins and co-workers [23,29] reported precursor particles in a range of 10 to 40 nm in diameter for diffusion flames. Compared with this size, the aggregates measured in this paper would appear to be at a later stage of growth.

3.2. Quantitative measurements

Fig. 9 shows the evolution of droplet diameter for both JP8 and JP8 + 100 fuels in the coordinates of the classical D^2 law. The evolution of droplet diameter for nonane and hexanol is also shown for comparison. The trends show that there is virtually no difference between the evaporation rate of JP8 and JP8 + 100.

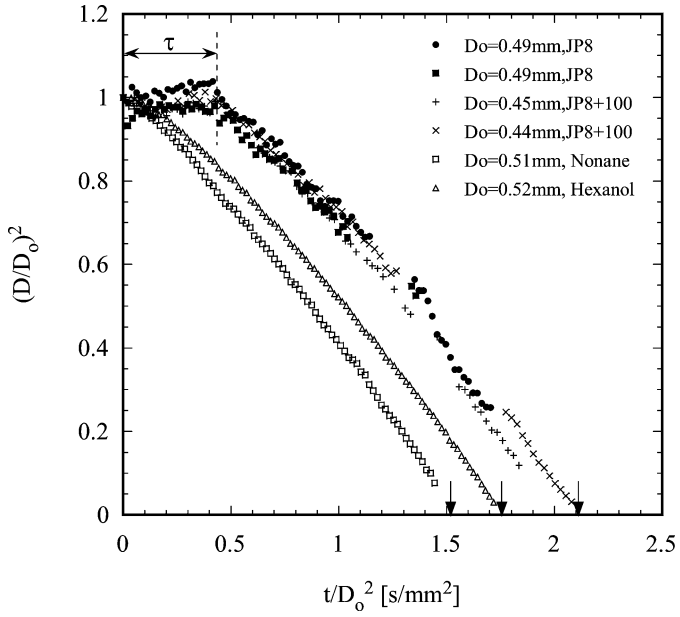

Fig. 9. Evolution of droplet diameter for JP8, JP8 + 100, nonane, and hexanol droplets burning in air. Droplet heating period is indicated as τ. Arrows identify the burning time, t_b.

This situation is consistent with an additive existing in trace quantities in a fuel.

JP8 and JP8 + 100 showed significant initial heating as indicated by the time τ in Fig. 9. On the other hand, nonane, hexanol, and JP8 + hexanol showed no evidence of droplet heating. Droplet heating is related to the thermal diffusion time, τ_{df},

$$\tau_{df} \approx \frac{D_o^2}{\alpha_l} \tag{1}$$

as [30]

$$\tau \approx \tau_{df} \frac{k_l}{k_g} \ln\left(\frac{T_f - T_\infty}{T_f - T_d}\right). \tag{2}$$

For the flame temperature we used the approximation of the adiabatic flame temperature [27] which, for present purposes, should be acceptable as it occurs in a logarithmic term and we are only interested in general trends for the direction τ takes as additives are introduced in the blend and the inert is changed (from nitrogen to helium). Property estimates were obtained from the literature data [31–35]. The results were sensitive to how k_g was computed. We used a mole fraction average k_g with weighting of 40% fuel vapor and 60% inert evaluated at $(T_f + T_d)/2$. From Eq. (2) over the temperature range 300 K $< T_d <$ 550 K we found the trend that $\tau_{JP8} > \tau_{hexanol,nonane,JP8+hexanol}$ and that $\tau_{helium\,mixture} < \tau_{nitrogen\,mixture}$, the latter being a consequence of the large increase of helium thermal conductivity compared to nitrogen. This trend is consistent with experimental results for air and the 70% He/30% O_2 mixture.

Despite its multicomponent nature, JP8 did not show evidence of preferential vaporization (see Fig. 9 and Fig. 12 later). This effect would typically be revealed by a "plateau" in the evolution of droplet diameter, similar to the droplet heating period that occurs immediately after ignition. In a highly multicomponent system like JP8, which has components with a range of heats of vaporization and boiling points, several species evaporate in parallel. As one becomes depleted another is still contributing significantly, which produces a time-dependent slope in the D^2 progressions.

With 50% hexanol added to JP8, the evaporation rate of the JP8 + hexanol mixture exhibits a remarkable similarity to pure hexanol and essentially reduces to it as shown in Fig. 10. This trend is further illustrated in Fig. 11 which shows the evolution of burning rate as the first derivative of the D^2 profiles, $K \equiv -d(D)^2/dt$, in Fig. 10. The derivatives were taken from data in Fig. 10 by a linear interpolation between adjacent data. The JP8 + hexanol and JP8 + 100 + hexanol mixtures are well within the scatter of the measurements for hexanol. The presence of hexanol at 50% in JP8 and JP8 + 100 seems to turn them into a blend that burns essentially like pure hexanol in terms of burning rate. This strong influence of hexanol in JP8 is contrasted with results for spherical droplet flames of hexanol mixed with nonane [13] where at 50% the mixture has a more typical behavior of being intermediate to the burning process of the components.

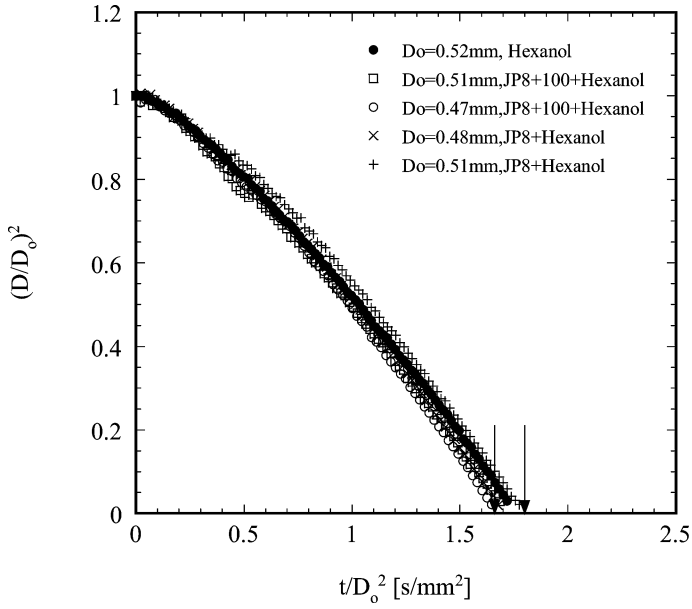

Fig. 10. Evolution of droplet diameter for JP8 + hexanol and JP8 + 100 + hexanol droplets burning in air. Arrows label the burning time, t_b.

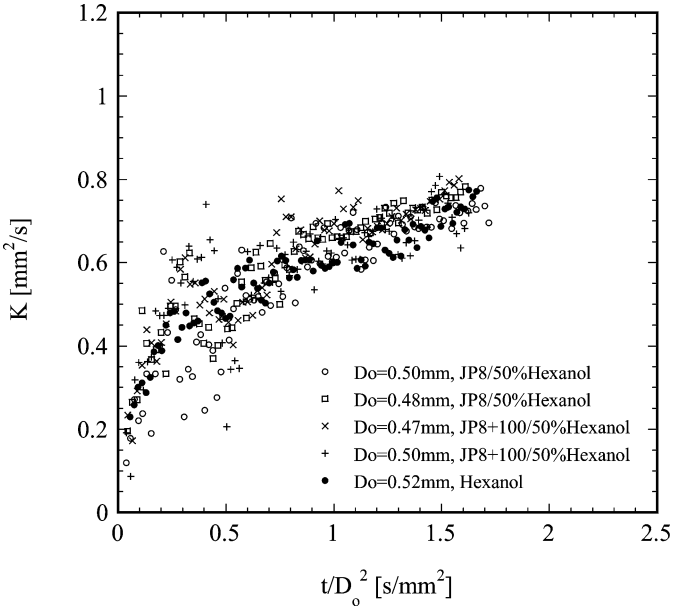

Fig. 11. Time-dependent burning rate for JP8 + hexanol, JP8 + 100 + hexanol (from Fig. 10), and pure hexanol droplets burning in air.

The burning rate increases with time for JP8 + hexanol in air shown in Fig. 11. Similar trends were noted in previous work for spherical droplet flames for the nonane/hexanol mixture [13]. This is counter to the classical D^2 burning process which predicts that K should be independent of time [36]. In the 70% He/30% O_2 mixture a time-dependent K also occurs as discussed below. Since a time-dependent burning rate occurs in the 70% He/30% O_2 mixture where no appreciable soot forms, as well as in air where soot formation is extensive, soot formation is discounted for this effect.

We believe that a time-dependent K is the result of a continually increasing droplet temperature and re-

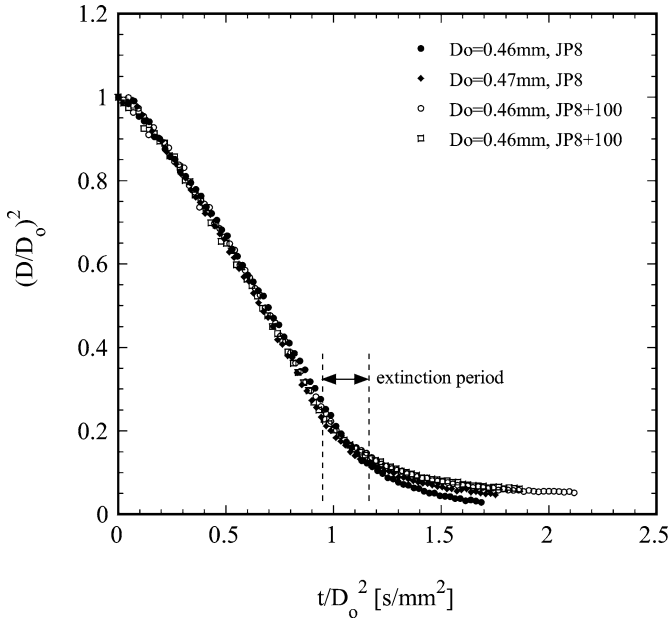

Fig. 12. Evolution of droplet diameter for JP8 and JP8 + 100 droplets burning in the 70% He/30% O_2 mixture. Extinction is indicated as the time where the flame disappears. Droplets continue to evaporate thereafter as the gas cools.

duction of liquid density even after $t > \tau$. Predictions of the droplet temperature [37] show that the droplet heating rate is steep immediately after ignition, which corresponds to the period τ, and is thereafter more gradual as the droplet temperature asymptotically approaches the wet bulb temperature of the fuel. The conjecture is that for $t > \tau$ the liquid density decreases at a much lower rate than for $t < \tau$ and that the change in density cannot compensate the evaporation of fuel to maintain a constant diameter in this domain. The result is an increasing burning rate throughout the burning process as shown in Fig. 11.

As noted previously, in the 70% He/30% O_2 mixture JP8 and JP8 + 100 droplets produce considerably less soot than they do in air and droplet visibility thereby increases which improves data quality and increases the density of measurements that can be made. Figs. 12 and 13 show the evolution of droplet diameter and burning rate, respectively, for JP8 and JP8 + 100 droplets burning in the 70% He/30% O_2 mixture. Differences between JP8 and JP8 + 100 are minimal which is consistent with the results for burning in air (Fig. 9) and the trace level of +100 in JP8. The significant droplet heating found for burning in air (Fig. 9) is completely absent for JP8 burning in the 70% He/30% O_2 mixture (Fig. 12). This is a consequence of the much higher gas-phase thermal conductivity of helium (about five times that of nitrogen) and enhanced heat transfer to the droplet compared to burning in air which combine to reduce τ. A manifestation of increased heat transfer to the droplet should also be a shorter overall burning time t_b (where $t_b = t(D \to 0)$) and this is consistent with Figs. 9 and 12, where $t_{b,\text{helium inert}} < t_{b,\text{nitrogen inert}}$. As a final point on the evolution of droplet diameter for burning in the 70% He/30% O_2 mixture related to Fig. 12, extinction was regularly observed for JP8 and JP8 + 100. Flame extinction is consistent with the lower flame temperature and greater heat losses (because of higher average gas thermal conductivity due to helium) that cannot sustain combustion. After extinction the JP8 droplet continues to evaporate and the diameter continues to decrease, though at a much slower rate as shown in Figs. 12 and 13. This effect is due to cooling of the gas after the flame extinguishes.

The evolution of flame standoff ratio, D_f/D, for JP8 burning in air and the 70% He/30% O_2 mixture is shown in Fig. 14. The flame standoff ratio is the ratio of flame diameter to instantaneous droplet diameter computed at each time by cross-referencing smoothed data from plots like those in Figs. 10 and 12. For either ambience there is no distinguishable difference of the flame position between JP8 and JP8 + 100 which further shows the minimal (if any) influence of +100 on the JP8 spherical flame combustion dynamic. This is consistent with an additive in trace quantities. There is a large difference of the flame standoff ratio for the nitrogen inert compared to the helium inert with $D_f/D|_{\text{helium}} > D_f/D|_{\text{nitrogen}}$. This trend can be understood in terms of increased gas-phase heat transport in helium, as compared to nitrogen. The mechanisms are the higher average gas thermal conductivity

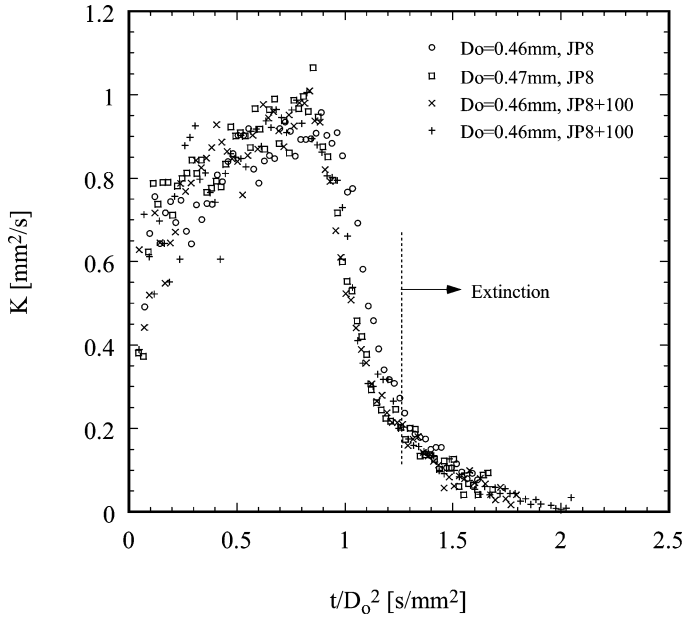

Fig. 13. Time-dependent burning rates (from data in Fig. 12) for JP8 and JP8 + 100 droplets burning in the 70% He/30% O_2 mixture.

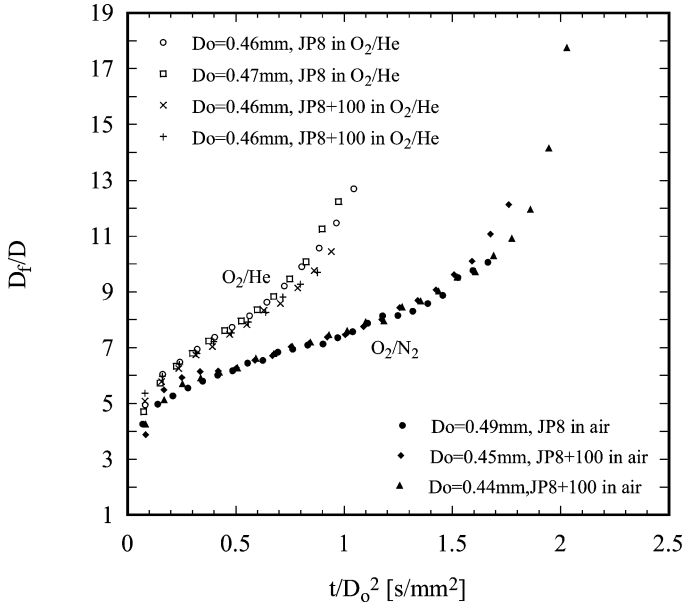

Fig. 14. Flame standoff ratios for JP8 and JP8 + 100 droplets burning in air and the 70% He/30% O_2 mixture.

in helium compared to nitrogen which would tend to position the flame farther away from the droplet in helium and a reduced flame temperature in helium which would tend to position the flame closer to the droplet. The former overrides the latter based on the trend shown in Fig. 14.

The soot shell standoff ratio in air, D_S/D, is shown in Fig. 15, where D_S is the measured soot shell diameter when an instantaneous diameter is measured. No soot shells were found for the 70% He/30% O_2 mixture or pure hexanol. The delay period when soot is forming and accumulating in the shell is indicated. The data show that the soot standoff positions are virtually indistinguishable for JP8, JP8 + 100, and JP8 + 100 + hexanol. On the other hand, the soot shell diameter for the nonane flame is significantly larger

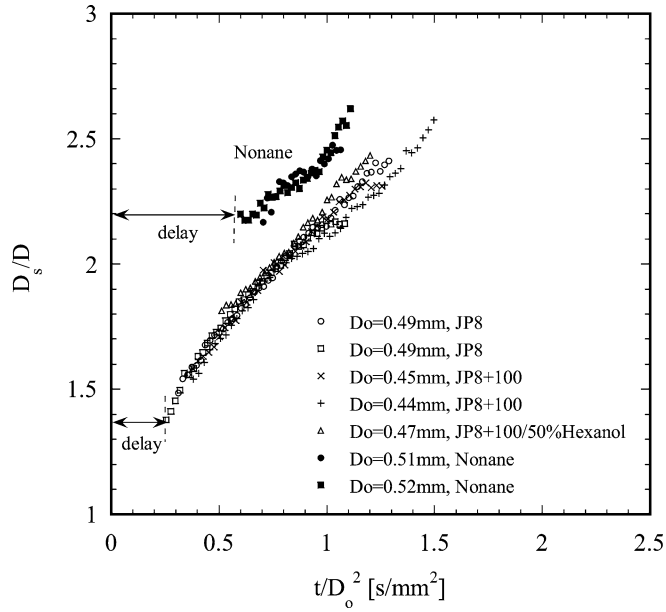

Fig. 15. Evolution of soot shell diameter for JP8, JP8 + hexanol, and nonane droplets burning in air. Delay period before appearance of soot shell is indicated.

than that for JP8. This is caused by the higher flame temperature of JP8 compared to nonane which would result in a higher thermophoretic velocity which traps aggregates closer to the droplet for nonane compared to JP8.

3.3. Correlation

The droplet, flame, and soot shell diameters each exhibit strong time dependencies which are significantly different from each other. We present a way to consolidate these measurements. There are two constraints: (1) a consistency condition for the soot standoff ratio is $1 < D_s/D < D_f/D$ for soot formation to be on the fuel-rich side of the droplet flame; and (2) the forces or velocity components on soot aggregates must balance. The forces are due to Stefan flow, thermophoresis, and diffusiophoresis [6–8,24]. Stefan flow and diffusiophoresis are outwardly directed toward the flame and thermophoresis acts toward the droplet [8].

Taking the case where thermophoresis dominates over diffusiophoresis, a scale analysis on the appropriate velocities shows that $(D_f - D_s)/D \propto t/D^2$ apart from a proportionality factor. A correlation for the present measurements based on these coordinates worked well for a given fuel but it did not correlate all of the measurements of the different blends we examined onto a single curve. We found in an ad hoc way that by plotting $(D_f - D_s)/(D_s - D)$ in terms of a scaled time, t/t_b, the data were better consolidated. Fig. 16 shows the measurements presented in this way for conditions where D_s could be measured. The data come from Figs. 9, 10, 14, and 15. A correlation of the data was obtained in the form

$$\frac{D_f - D_s}{D_s - D} = C \cdot \left(\frac{t}{t_b}\right)^n, \tag{3}$$

where C and n are correlation coefficients with the values $C = 3.47$ and $n = -0.43$. The utility of such a correlation is that it provides a means to predict the evolution of D_s given the droplet and flame diameter. At the present time, the correlation is assumed to be applicable only for data of given initial droplet diameter in the range examined here.

4. Conclusions

The following results and conclusions are drawn from this study.

(1) The burning rates, flame standoff ratios, and soot shell standoff ratios of JP8 and JP8 + 100 are indistinguishable.
(2) The flame standoff distance for JP8 burning in the 70% He/30% O_2 mixture was larger than that for burning in the nitrogen mixture (air) showing the dominance of a higher average gas thermal conductivity over a lowered flame temperature.
(3) The photographic evidence of JP8 + 100 and JP8 droplet flames suggested some reduction of sooting tendency of JP8 + 100 compared to JP8, though this result needs further study for

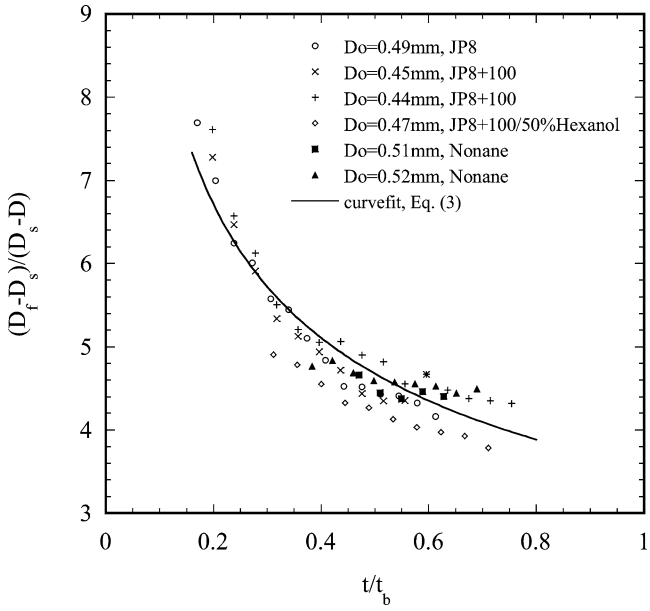

Fig. 16. Scaling of droplet, flame, and soot shell diameters with time scaled by the droplet burning time, t_b. Data are only included where soot shell and droplet could be clearly seen.

generalization. In the 70% He/30% O_2 mixture, the JP8 + 100 flames were almost entirely blue while JP8 flames showed a very distinctive yellow emission.

(4) Much less soot accumulates in the soot shell for JP8(+100) + 50% hexanol compared to JP8 or JP8 + 100. Sooting trends in the relationship JP8 > JP8 + 100 > JP8(+100) + hexanol are inferred from the photographic documentation of the droplet burning process reported in this paper.

(5) JP8 and JP8 + 100 showed significant droplet heating characterized by a near constant droplet diameter for almost 20% of the droplet lifetime. Droplet heating was virtually eliminated by blending JP8 with 50% hexanol and/or burning in a helium inert, which was due to enhanced heat transfer to, and within, the droplet associated with hexanol addition (and its higher liquid thermal diffusivity) and substitution of nitrogen with helium in the oxidizing ambience (and helium's much higher thermal conductivity compared to nitrogen).

(6) The burning rates of JP8 + 50% hexanol are nearly the same as those of pure hexanol showing the dominance of hexanol on the JP8 droplet burning process.

(7) Nonlinear burning characterized by a time-dependent burning rate was observed for all of the JP8 droplet blends examined, as well as for pure hexanol and nonane. It is most probably not the result of soot formation because nonlinear burning was found for burning in air where soot formation is extensive as well as for burning in the 70% He/30% O_2 mixture where soot formation was almost completely eliminated.

(8) The flame and soot standoff ratios of JP8, JP8 + hexanol blends, and nonane showed a reasonable correlation when presented with the coordinates $(D_f - D_s)/(D_s - D)$ and t/t_b.

Acknowledgments

We thank Dr. Edward Owens of Southwest Research Institute (San Antonio, TX) for supplying the JP8 used in our study and for helpful discussions and Brian J. Callahan, Daniel J. Catropa, Radford J. Fagan, and Messrs. Darius Liu for their help with the experiments. Conversations with Dr. Wing Tsang of the NIST are greatly appreciated. This research was supported by the National Aeronautics and Space Administration, NAG 3-2224 (Dr. Daniel Dietrich as Project Monitor and Dr. Merrill King as Program Director).

References

[1] T. Edwards, L.Q. Maurice, J. Prop. Power 17 (2001) 461–466.

[2] S.P. Heneghan, S. Zabarnick, D.R. Ballal, W.E. Harrison, J. Energy Resour. Technol. 118 (1996) 170–179, also AIAA Paper No. 96-0403.

[3] S.P. Heneghan, T.F. Williams, C.R. Martel, D.R. Ballal, J. Eng. Gas Turbines Power 115 (1993) 480–484.
[4] J.C. Yang, G.S. Jackson, C.T. Avedisian, Proc. Combust. Inst. 23 (1991) 1361–1367.
[5] G.S. Jackson, C.T. Avedisian, Proc. R. Soc. London Ser. A 446 (1994) 257–278.
[6] G.S. Jackson, C.T. Avedisian, J.C. Yang, Int. J. Heat Mass Transfer 35 (8) (1992) 2017–2033.
[7] C.T. Avedisian, in: Physical and Chemical Aspects of Combustion, Gordon & Breach, New York, 1997, pp. 135–160, Chapter 6.
[8] G. Ben-dor, T. Elberin, B. Krasovitov, Proc. R. Soc. London Ser. A 459 (2003) 677–703.
[9] G.S. Jackson, C.T. Avedisian, Combust. Sci. Technol. 115 (1996) 127–147.
[10] B.D. Shaw, A.G. Chen, Microgravity Sci. Technol. 10 (3) (1997) 136–143.
[11] G.J. Green, T.Y. Yan, D.Y. Goswami, in: Proc. 23rd Intersociety Energy Conv. Eng. Conf., vol. 1, 1988, pp. 291–296.
[12] B.J. Wood, H. Wise, S.H. Inami, Combust. Flame 4 (1960) 235–242.
[13] C.T. Avedisian, B.J. Callahan, Proc. Combust. Inst. 28 (2000) 991–997.
[14] W.A. Sirignano, Fluid Dynamics and Transport of Droplets and Sprays, Cambridge Univ. Press, Cambridge, UK, 1999, pp. 7, 280.
[15] S.S. Sadhal, J.N. Chung, P.S. Ayyaswamy, Transport Phenomena with Drops and Bubbles, Springer-Verlag, New York, 1997, pp. 181–182.
[16] H.J. Curran, E.M. Fisher, P.A. Glaude, N.M. Marinov, W.J. Pitz, C.K. Westbrook, D.W. Layton, P.F. Flynn, R.P. Durrett, A.O. zur Loye, O.C. Akinyemi, F.L. Dryer, SAE Paper No. SAE-010653, 2001.
[17] G.S. Jackson, C.T. Avedisian, J.C. Yang, Proc. R. Soc. London Ser. A 435 (1991) 359–368.
[18] E. Owens, Southwest Research Institute, San Antonio, TX, private communication, October 10, 2001.
[19] C.T. Avedisian, J.C. Yang, C.H. Wang, Proc. R. Soc. London Ser. A 420 (1988) 183–200.
[20] P.M. Struk, D.L. Dietrich, J.S. T'ien, Microgravity Sci. Technol. 9 (1996) 106–116.
[21] C.T. Avedisian, J. Prop. Power 16 (4) (2000) 628–635.
[22] C.T. Avedisian, G.S. Jackson, J. Prop. Power 16 (6) (2000) 974–979.
[23] C.M. Megaridis, R.A. Dobbins, Combust. Sci. Technol. 66 (1989) 1–16.
[24] M.Y. Choi, F.L. Dryer, G.J. Green, J.J. Sangiovanni, 31st Aerospace Sciences Meeting & Exhibit, Reno, NV, AIAA Paper No. 93-0823.
[25] K.C. Salooja, J. Inst. Fuel 45 (1972) 37–42.
[26] B.S. Haynes, H. Jander, H. Mätzing, H.G.G. Wagner, Combust. Flame 40 (1981) 101–103.
[27] P.A. Bonczyk, Combust. Flame 87 (1991) 233–244.
[28] B.S. Haynes, H.G.G. Wagner, Prog. Energy Combust. Sci. 7 (1981) 229–273.
[29] R.A. Dobbins, Combust. Flame 130 (2002) 204–214.
[30] A.T. Kanury, Introduction to Combustion Phenomena, Gordon & Breach, New York, 1975, pp. 191–192.
[31] W.C. Reynolds, "STANJAN," Dept. Mech. Eng., Stanford, CA, 1986.
[32] R.C. Reid, J.M. Prausnitz, B.E. Poling, The Properties of Gases and Liquids, McGraw–Hill, Boston, 1987, p. 515, Appendix A.
[33] C.K. Law, F.A. Williams, Combust. Flame 19 (1972) 393–405.
[34] Coordinating Research Council Report No. 530, Coordinating Research Council, Atlanta, GA, 1983.
[35] T.E. Daubert, R.P. Danner, Physical and Thermodynamic Properties of Pure Chemicals: DIPPR (Design Institute for Physical Property Data) Project 801 Evaluated Process Design Data, Greyden Press, Columbus, OH, San Diego, 1999.
[36] I. Glassman, Combustion, third ed., Academic Press, San Diego, 1996, pp. 285–287, 298.
[37] W.A. Sirignano, C.K. Law, Adv. Chem. 166 (1978) 3–26.